Preprints of the 19th World Congress
The International Federation of Automatic Control
Cape Town, South Africa. August 24-29, 2014

A Nonlinear Input Shaping Technique for Motion Control of a Sensing Antenna

Feliu-Talegón D., Feliu-Batlle V., Castillo-Berrio C.F.

Escuela Técnica Superior de Ingenieros Industriales, Universidad de Castilla-La Mancha, Campus Universitario s/n, Ciudad Real, 13071, Spain (Tel: 34 926295364; e-mail: Vicente.Feliu@uclm.es)

Abstract: Flexible links combined with force and torque sensors can be used to detect obstacles in mobile robotics, as well as for surface and object recognition. These devices, called sensing antennae, perform an active sensing strategy in which a servomotor system moves the link back and forth until it hits and object. At this instant, information of the motor angles combined with force and torque measurements allow calculating the positions of the hitting points, which are valuable information about the object surface. In order to move the antenna fast and accurately, this article proposes a new open loop control for driving this flexible link based sensor. The control strategy is based on an (*IS*) Input Shaping technique, in order to reduce link vibrations. The antenna performs free azimuthal and vertical movements. However, the vertical movement is clearly non-linear due to the gravity effect, which prevents the use of standard linear *IS* techniques. Then a new nonlinear *IS* has been developed in this article which includes a linearization term of the gravity. Experiments have shown the improvements attained with this technique in the accurate and vibration free motion of our antenna.

Keywords: Input shaper, antenna sensor, flexible link, nonlinear system, linearization technique.

1. INTRODUCTION

Obstacle detection and object recognition can be approached by using optical sensors, as computer vision, but they may fail when illumination is inappropriate or when fog, darkness, glare and reflections are present. Besides, flexible links combined with force and torque sensors can also be used to detect obstacles in mobile robots, as well as for 3D object recognition, while avoiding these drawbacks. These devices, called sensing antennae, perform an active sensing strategy in which a servomotor system moves the link back and forth until it hits and object. At this instant, information of the motor angles combined with force and torque measurements allow calculating the positions of the hit points, which are valuable information about the object surface. By repeating this operation, a 3D map of the surface of an object can be obtained which allows its recognition. Moreover, information about the texture of the object surface can also be detected with these devices (Prescott and Pearson (2009)).

The antenna sensor is composed of two parts: 1) a sensing element which may be a loadcell or a (F-T) force and torque sensor and 2) the flexible-link attached by one of its ends to the top of the sensing element. Some prototypes of antennas for active touch have been developed by Ueno et al. (1996), Kaneko et al. (1998), Scholz and Rahn (2004), and Zhao and Rahn (2010). In the first two works, the contact point was calculated from the frequencies obtained by processing the vibrations that appeared in the mechanical structure as a consequence of the impact. In other works, e.g. Scholz and Rahn (2004), only the link static deflection was considered. The equation of the elastica yielded a highly nonlinear kinematic differential equation that allowed obtaining the contact point from angle and force measurements.

If the control system does not consider link elasticity, residual vibrations may appear that prevent the accurate and fast approach to the target points to be searched. Moreover, permanent collisions with the object could happen, where the link hits back and forth, which would produce delays in the recognition process and reduce the quality of the estimates of the object surface. However, none of the previous works studied the control of the free motion of antennas. Instead they focused on the contact force control once the antenna has hit the object. In this case, position control was achieved in a direction while the force normal to the contact surface was controlled, e.g. Zhao and Rahn (2010).

We have carried out some previous research on position control of antennas: in Castillo et al. (2011a) the link of a robotic antenna was modeled assuming a lumped mass model, in Castillo et al. (2011b) the vibrations of the antenna flexible-link were reduced using an open-loop control based on the dynamic inversion, and in Feliu et al. (2013) the vibrations of the antenna were reduced using a simpler open-loop control based on the input shaping technique (*IS*). As *IS* are filters designed to remove vibrations in linear systems (the method relies in the additive property of these systems), and our antenna is highly nonlinear, this control did not perform too well in trajectories that involved elevation movements. Then this article improves the previous one by developing a new nonlinear input shaper filter that significantly reduces the residual vibrations that appear after having performed a fast movement with the antenna.

* This study was supported by the Spanish Ministry of Economy and Competitiveness and by the European Social Fund with project DPI2012-37062-CO2-01.

The link used in our platform is very flexible and the dynamics of the system is represented by a nonlinear highly coupled multivariable model of 8th order. Our control system has to perform two control tasks: 1) motor positioning and 2) tip positioning trying to get rid of the permanent oscillation. In this work, motor positioning is achieved by closing high gain loops around the joints in order to control their angular positions and compensate for friction. Algebraic controllers were therefore designed following the methodology described in Castillo et al. (2011b).

Tip positioning cannot be easily achieved as the antenna link vibration modes are difficult to remove because: 1) the link vibration frequencies are high, 2) motors have a limited bandwidth, and 3) a relatively cheap real-time computer system with low sampling rate is used. These three issues led us to apply open loop instead of closed loop control techniques in order to remove the vibrations. Then, as mentioned before, we propose an open loop control strategy which is based on the well known *IS* technique to reduce the vibrations of flexible links. The standard *IS* technique has been explained in Singer and Seering (1990), and Huey et al. (2008), and consists in generating a command reference that does not excite the vibration modes of the link. It generates command references for the motors by passing the desired tip trajectory through a finite impulse response (FIR) filter. The main problem for the *IS* technique is dealing with system uncertainties produced by model errors or changes in the system parameters. In order to solve it, robust, learning and adaptive approaches have been proposed, such as in Park and Chang (2001), and Pereira et al. (2009). *IS* techniques are only suited for linear time-invariant systems while our antenna is highly non-linear. Then, this research develops a new nonlinear *IS* for reducing the antenna tip vibrations. This paper is organized as follows. Section 2 presents our antenna prototype. Section 3 proposes a simplified dynamic model of the link. Section 4 develops the proposed motion control system. Experimentation of the control system is described in Section 5, and Section 6 presents some conclusions.

2. THE EXPERIMENTAL ANTENNA

The proposed sensing antenna consists of a flexible-link attached by one of its ends to a sensor holder (loadcell), and two DC mini servo actuators PMA-5A motor sets (from Harmonic drive which include reduction gears and incremental encoders) that move the loadcell. The setup is shown in Figure 1. The loadcell is an ATI Mini 40 force-torque sensor with a transducer hardware and a digital card NI PCI-6220 for data acquisition. The system runs under Microsoft Windows XP 2002, INTEL Core (TM) 2 Quad CPU, Q8200 2.33 GHz, 3 GB of RAM. The data acquisition and control algorithms are programmed using Labview 7.1. The sampling time of the system data acquisition (measurements and control signals) is T=0.004 s.

2.1 Antenna Features.

The workspace of the two Degrees of Freedom (2DOF) antenna is spherical and is composed of azimuthal and attitude movements. In Figure 2, the tip position is expressed in spherical coordinates ϕ_1 and ϕ_2, the motor angles are θ_1 and θ_2, and subscripts 1 and 2 mean respectively azimuthal and attitude angles. The antenna features are listed in Table 1, where *E* is the Young's modulus, *I* is the inertial moment of the flexible link cross section, *r* is the link radius, m_d is the link mass and l = 1 m is the link length which has been determined by the desired workspace dimension.

Fig. 1. Experimental platform.

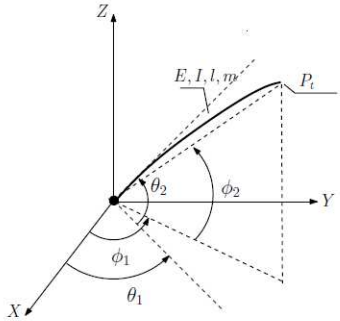

Fig. 2. Flexible-link schematic model.

Table 1. Flexible-link Characteristics.

Feature	Quantity	Unit
l	1	m
r	0.001	m
m_d	$4.54 \cdot 10^{-3}$	kg
E	$1.15 \cdot 10^{11}$	N/m^2
I	$7 \cdot 10^{-5}$	m^4

3. DYNAMIC MODEL OF THE LINK

The antenna dynamics has been modelled assuming distributed masses along the flexible link. Usually, the resulting infinite high-order dynamics is approximated by a truncated model of finite order. Consider a flexible-link which rotates in a horizontal plane (an azimuthal movement without gravity effects). In this case, the vibration frequencies of a link with pinned-free ends can be obtained as the solutions of the equation:

$$\cos(\beta_i \cdot l) \cdot \sinh(\beta_i \cdot l) - \sin(\beta_i \cdot l) \cdot \cosh(\beta_i \cdot l) + \frac{J}{\rho} \beta_i^2 \cdot (1 + \cos(\beta_i \cdot l) \cdot \cosh(\beta_i \cdot l)) = 0 \quad (1)$$

where J is the rotational motor inertia referred to the link side and ρ is the linear mass density ($\rho=m_d / l$). Every solution β_i, $1 \le i < \infty$ of the previous characteristic equation yields an associate vibration angular frequency

$$\omega_i = \beta_i^2 \sqrt{E \cdot I / \rho} \tag{2}$$

Vibration frequencies of a link with clamped-free ends can also be obtained from (1) by taking its limit if $J \to \infty$. In this case, (1) becomes $\cos(\beta_i \cdot l) \cdot \cosh(\beta_i \cdot l) = -1$ which, combined with (2), yields the required angular frequencies. Simulation of the movements considering the flexible-link parameters of Table 1, as well as experimentation, showed that:

- Only the vibration modes associated to the two lowest frequencies (ω_1 and ω_2) were noticeable.
- The mode of the lowest frequency (ω_1) was much more significant in the time response of the tip than the mode of the second frequency (ω_2).
- The above items are valid both for flexible-links with pinned-free ends and clamped-free ends.

Then the dynamic model of the link is truncated considering a single vibration mode yielding the linear model

$$\frac{\phi_1(s)}{\theta_1(s)} = \frac{237.63 - 0.1386 \cdot s^2}{s^2 + 237.63}; \quad \frac{\Gamma_1(s)}{\theta_1(s)} = \frac{0.3586 \cdot s^2}{s^2 + 237.5} \tag{3}$$

where Γ_1 is the torque at the base of the link in the azimuthal rotation direction, which can be measured by the force-torque sensor.

Let us assume a massless link with the same mechanical features of our link (E, I and l) but having a lumped mass m at the tip. In order to make this link equivalent to the actual one, the equivalent tip mass can be calculated as the value that yields the same rotational inertia as the actual link. This condition establishes that $m = \rho \cdot l / 3 \approx 1.51 \cdot 10^{-3}$ kg.. The dynamic model of this equivalent link can be easily determined:

$$\frac{\phi_1(s)}{\theta_1(s)} = \frac{237.5}{s^2 + 237.5}; \quad \frac{\Gamma_1(s)}{\theta_1(s)} = \frac{0.3586 \cdot s^2}{s^2 + 237.5} \tag{4}$$

It can be noticed that models (3) and (4) are very similar. The main difference is that the actual link is non-minimum phase and the equivalent lumped model is minimum phase. But we have verified that the effect of the s^2 term of the numerator of ϕ_1 / θ_1 (which has zeros in ± 41.41) in the dynamics of the actual link (3) is very small, and it can be neglected.

Based on the previous analysis, we assume that our sensing antenna can be modelled as a massless flexible link with a lumped mass at its tip. Then a relatively simple nonlinear multivariable model can be obtained for our 2 DOF antenna with azimuthal and attitude movements (Castillo et al. (2011a)):

$$m \cdot l^2 \cdot \cos^2(\phi_2) \cdot \ddot{\phi}_1 - m \cdot l^2 \cdot \sin(2 \cdot \phi_2) \cdot \dot{\phi}_1 \cdot \dot{\phi}_2 = \frac{3 \cdot E \cdot I}{l} \cos(\phi_2) \cdot \cos(\theta_2) \cdot \sin(\theta_1 - \phi_1) \tag{5}$$

$$m \cdot l^2 \cdot \ddot{\phi}_2 + \frac{m \cdot l^2}{2} \cdot \sin(2 \cdot \phi_2) \cdot \dot{\phi}_1^2 + m \cdot g \cdot l \cdot \cos(\phi_2) = \frac{3 \cdot E \cdot I}{l} [\cos(\phi_2) \cdot \sin(\theta_2) - \sin(\phi_2) \cdot \cos(\theta_2) \cdot \cos(\theta_1 - \phi_1)] \tag{6}$$

where the inputs are θ_1 and θ_2, and the outputs ϕ_1 and ϕ_2.

Tip angles can be estimated from motor angles and torque measurements provided by the force-torque sensor using the approximate expression:

$$\phi_i^e = \theta_i - \Gamma_i \cdot l / (3 \cdot E \cdot I), \quad i = 1,2 \tag{7}$$

where Γ_i are the torques measured by the sensor in the directions corresponding to the degees of freedom of θ_1 and θ_2 (more details can be found in Castillo et al (2014)).

4. CONTROL SYSTEM

The control system has two components. The first one consists of the closed loop control of the two motor positions (angles θ_1 and θ_2), and the second one is the open loop control of the tip position (angles ϕ_1 and ϕ_2). The first component is only briefly described here because it was developped in previous papers. The second component is developed here in detail because it is the object of the present research.

4.1 Motor Control.

Motor control was implemented using PID controllers with a low pass filter term. They ensure good trajectory tracking, compensate disturbances such as nonlinear Coulomb friction or unmodelled components of the friction, and are robust to parameter uncertainties, providing precise and fast motor positioning responses.

The scheme with two degrees of freedom shown in Figure 3 is used for the motor control. In this scheme, $n_{1,i}(s)$, $n_{2,i}(s)$ and $d_i(s)$ are second order polynomials, having $d_i(s)$ a root at the origin in order to remove steady state errors to input commands and disturbances. V_i are the motor control signals, θ_i^* are the motor references, θ_i are the actual motor angles and $G_{m,i}(s)$ are the motor transfer functions. We assumed that the dynamics of each motor were decoupled from the remaining of the mechanical structure since we use gears with high reductio ratios (n = 100).
The four closed loop poles of this scheme can be arbitrarily placed following an algebraic method described in Castillo et

al. (2011b). All the closed loop poles of each motor were placed in the same location p_i. Values $p_1 = -60$ and $p_2 = -70$ were chosen. Moreover, polynomials $n_{1,i}(s)$ and $n_{2,i}(s)$ were designed in order to cancel the two zeros of the closed loop motor transfer functions with two of its poles, and make the unity the gains of these transfer functions. Then the transfer functions $M_i(s)$ of the closed loop motors are:

$$\frac{\theta_i(s)}{\theta_i^*(s)} = M_i(s) = \frac{1}{(1+\alpha_i \cdot s)^2}, \quad \alpha_i = -p_i^{-1} \tag{8}$$

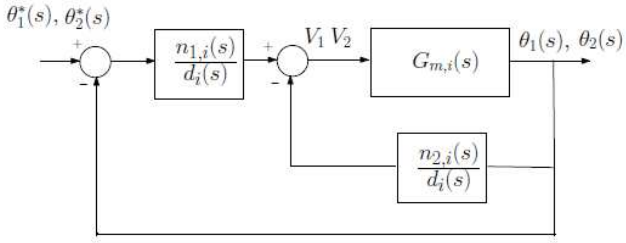

Fig. 3. Algebraic motor controller.

4.2 IS Technique.

The *IS* is a well known feedforward technique used to reduce vibrations produced when moving flexible structures. This technique basically removes the frequency components of the reference signal that could excite the vibration modes. It acts as a bandstop filter at the vibration frequencies of the link. Details about the foundations and refinements of this technique can be found in the references cited in the Introduction. We propose to use two *IS* filters, $IS_1(s)$ and $IS_2(s)$, which are respectively responsible of removing the vibrations in the azimuthal ϕ_1 and attitude ϕ_2 degrees of freedom of the tip. Each filter acts independently of the other. The input of each *IS* filter is the command trajectory of the corresponding tip degree of freedom (ϕ_1^* or ϕ_2^*), and each one yields as output the reference for the corresponding motor (θ_1^* or θ_2^*).

We consider the general robust *IS* structure for removing one vibration mode:

$$IS^{(q)}(s) = \left(0.5 \cdot (1 + e^{-\frac{\pi}{\omega_1} s}) \right)^q \tag{9}$$

where ω_1 is the vibration frequency of the link and q is the robustness index of the *IS*. We use the $IS^{(2)}$ configuration of (9), which is robust to limited variations of the vibration frequency. This *IS* has been chosen because the vibration frequency slightly changes with the attitude angle in the vertical movement as consequence of the nonlinearity introduced by gravity. Figure 4 shows the frequency responses of filters $q=1$ and $q=2$, and expresses the sensitivity function of each *IS*. The vertical axis is the normalized vibration amplitude, which is the ratio of the shaped to the unshaped vibration amplitudes, expressed as a percentage. The horizontal axis is the normalized frequency obtained by dividing the actual angular frequency of the system ω by the angular frequency ω_1 of the model. A level of vibration tolerance of 5% was defined for our application, which is also shown in Figure 4.

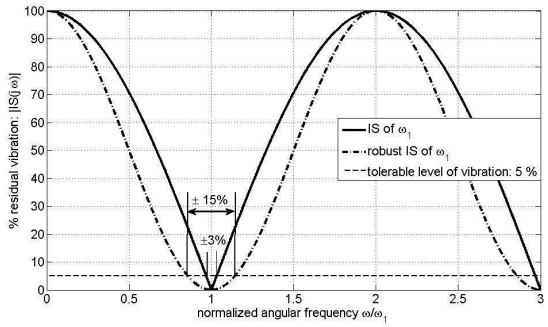

Fig. 4. Sensitivity functions of the *IS*.

The sensitivity curves of Figure 4 show that as the system frequency deviates from the design frequency, the amount of residual vibration increases rapidly. It also shows that $IS^{(2)}$ is a shaper more robust to modelling errors than $IS^{(1)}$. $IS^{(2)}$ is synthesized by forcing the derivative of the *IS* frequency response to be zero at the modelled frequency ω_1. This constraint maintains the vibration at a low level, even when there are modelling errors. Assuming a tolerable residual vibration lower than 5%, the allowed error in the modelled vibration frequency is of $\pm 3\%$ or $\pm 15\,\%$, depending on if the $IS^{(1)}$ or the $IS^{(2)}$ were respectively used. A variation of about $\pm 15\,\%$ of the nominal frequency in function of the attitude angle was detected. Then $IS^{(2)}$ filters have been used in this work. Otherwise, using q>2 does not further increase the performance but slows down the response.

4.3 New nonlinear IS Technique.

We make two simplifying assumptions in model (5), (6):

1. The Coriolis torque of (5) and the centripetal torque of (6) are much smaller than the corresponding inertial torques, and they can therefore be neglected. However the gravitational torque is significant in equation (6). Figure 5 illustrates this in a case of tracking a fast trajectory (simultaneous motion of angles θ_1 and θ_2 from 0^o to 45^o in a stepwise acceleration motion that lasts 1.2 s and the reference remains subsequently steady) with only closed loop motor control.
2. Link deflection is small which implies:

$$\sin(\theta_i - \phi_i) \approx \theta_i - \phi_i,\ \cos(\theta_i - \phi_i) \approx 1 \text{ and } \frac{\cos(\theta_i)}{\cos(\phi_i)} \approx 1.$$

If these two assumptions were verified, the model (5), (6) would become

$$\ddot{\phi}_1 + \omega_1^2 \cdot \phi_1 = \omega_1^2 \cdot \theta_1 \tag{10}$$

$$\ddot{\phi}_2 + \omega_1^2 \cdot \phi_2 + \frac{g}{l}\cos(\phi_2) = \omega_1^2 \cdot \theta_2 \tag{11}$$

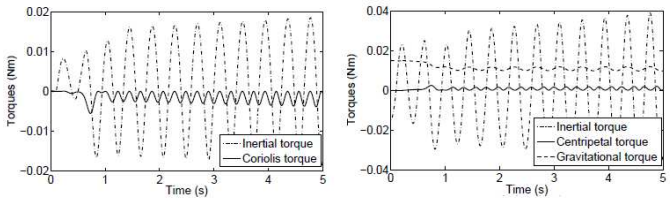

Fig. 5. Torques in equations (5) and (6) respectively.

being $\omega_1^2 = 3 \cdot E \cdot I /(m \cdot l^3)$. The first equation is linear and standard *IS* filters (9) could be used. The second equation is non linear because of the gravitational term. However we propose its linearization by defining the fictitious input:

$$\hat{\theta}_2 = \theta_2 - \frac{g}{l} \cdot \frac{\cos(\theta_2)}{\omega_1^2} = f(\theta_2) \tag{12}$$

in which we have assumed that $\cos(\theta_2) \approx \cos(\phi_2)$. Then equation (11) becomes

$$\ddot{\phi}_2 + \omega_1^2 \cdot \phi_2 = \omega_1^2 \cdot \hat{\theta}_2 \tag{13}$$

and standard *IS* filters could be used now. Figure 6 shows the complete feedforward control scheme of ϕ_2. The proposed linearization is not exact because the closed loop motor dynamics (8) are involved in the process, as Figure 6 shows. But it is easy to prove that this linearization would be very approximate if $\omega_1 << |p_2|$. In our case we have that $\omega_1 = 16.34$ rad/s. Then $|p_2|/\omega_1 = 4.3$, which approximately fulfills this condition and allows us to expect a good performance of our filter. In any case, this issue will be verified by the following experiments.

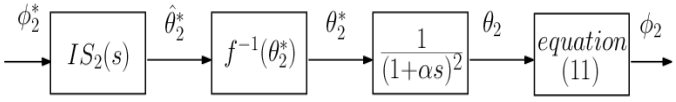

Fig. 6. Nonlinear *IS* filter of ϕ_2.

5. EXPERIMENTAL RESULTS

First, an attitude motion of 45º in 1.2 s was carried out. Figure 7 shows ϕ_2^*, and ϕ_2 in two cases: when only motor control is used and when motor control combined with $IS^{(2)}$ is used. In all the cases, tip angles are estimated by applying (7). Figure 8 shows ϕ_2 when motor control combined with our nonlinear $IS^{(2)}$ is used. The response with only motor control is drawn again for comparison purpose. Figure 9 shows the bending moments at the base of the link in this last experiment. Table 2 shows data of the amplitudes A_v of the residual vibrations obtained in this elevation motion. In this table, μ is the ratio between the residual amplitudes obtained using IS plus motor control and using only motor control.

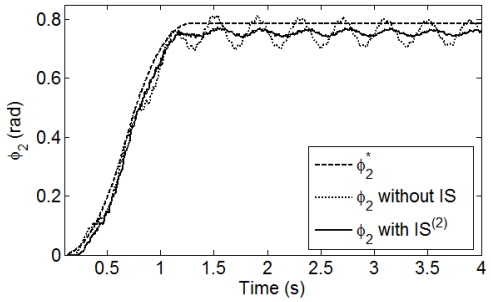

Fig. 7. Attitude movement using a standard $IS^{(2)}$.

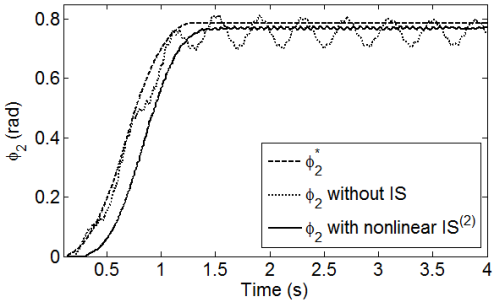

Fig. 8. Attitude movement using our nonlinear $IS^{(2)}$.

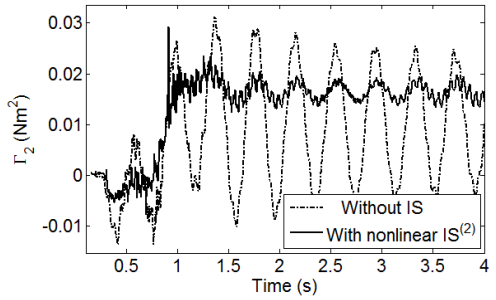

Fig. 9. Torque at the base of the link in the attitude movement using our nonlinear $IS^{(2)}$.

Table 2. Vibration reduction in an attitude motion.

Filter	A_v (mm)	Reduction ratio μ (%)	Rising time (s) (from 0 to 90% of the steady state)
No IS	57.8		0.92
$IS^{(2)}$	17.45	30.2	0.93
$IS^{(2)}$ with linearization	9.6	16.6	1.05

The combined azimuthal-attitude manoeuvre described in the first assumption of Section 4.3 was subsequently executed. Figures 10 and 11 show the experimental 3D trajectories of the antenna tip (estimated by applying (7) to obtain angles ϕ_1^e, ϕ_2^e and the subsequent calculation of the direct kinematic transformation) when motor control is applied to the two joints combined with: 1) no vibration control, 2)

$IS^{(2)}$ in both joints and 3) $IS^{(2)}$ in both joints and the scheme of Figure 6 in the second joint. These figures illustrate the projection of these 3D trajectories on a plane which is tangent to the antenna workspace sphere at a point which is the desired target of the antenna manoeuvre. The residual vibration can be observed in the upper left corner of these figures. Figure 11b shows the control signals involved in our nonlinear IS. Table 3 presents data of the amplitudes A_v of the residual vibrations obtained with this motion.

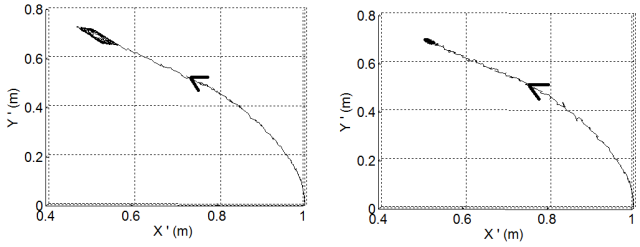

(a) (b)

Fig. 10. Projection of tip trajectories with: a) only motor control and b) motor control with $IS^{(2)}$ control in both joints

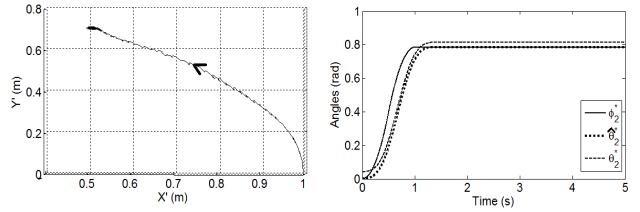

(a) (b)

Fig. 11. a) Projection of tip trajectory with motor control, linear $IS^{(2)}$ in the azimuthal angle and nonlinear $IS^{(2)}$ in the attitude angle, b) control signals of the scheme of Figure 7.

Table 3. Vibration reduction in a combined motion.

Filter ϕ_1	Filter ϕ_2	A_v (mm)	Reduction ratio μ (%)
No IS	No IS	59.2	
$IS^{(2)}$	$IS^{(2)}$	18.7	31.6
$IS^{(2)}$	$IS^{(2)}$ with linearization	16.9	28.5

6. CONCLUSIONS

A 2DOF flexible sensing antenna has been built. A combined motor position closed loop control – link vibrations open loop control has been proposed to improve the precision and the amount of the data collected by the antenna sensor.

A new nonlinear IS filter has been proposed to cope with the nonlinearity caused by gravity in attitude movements. Several experiments using *IS* schemes proved that our new IS significantly outperformed the standard linear $IS^{(2)}$. They illustrated that fast movements were achieved using our non linear $IS^{(2)}$ while reducing the tip vibration to about 50% of the value attained with a linear $IS^{(2)}$ in an attitude movement (Table 2). However, the reduction is smaller in a combined movement because the residual vibration in the azimuthal direction is logically not affected by our filter (Table 3). In any case, Figs. 7-11 show the effective reduction of the residual vibration amplitude attained using our filters. Finally, it can be noticed, comparing the permanent regimes of responses of Figs. 7 and 8, that our IS also reduces the steady state error caused by gravity in attitude motions.

REFERENCES

Castillo, C.F., Castillo, F.J. and Feliu, V. (2011a). Experimental Validation of 2 degrees of freedom whisker sensor dynamic model. *IFAC World Congress*, vol.18, Part 1, 3148-3152, 10.3182/20110828-6-IT-1002.02360, Milan, Italy.

Castillo, C.F., Castillo, F.J. and Feliu, V. (2011b). Inverse dynamics feed forward based control of two degrees of freedom whisker sensor. *IEEE International Conference on Mechatronics (ICM)*, 684-689, doi: 10.1109/ ICMECH.2011.5971202, Istanbul, Turkey.

Castillo, C.F., Engin, S.N. and Feliu, V. (2014). Design, Dynamic Modelling and Experimental Validation of a 2DOF Flexible Antenna Sensor, *International Journal of Systems Science*, 45(4), 714-727.

Feliu, D., Castillo, C.F., and Feliu V. (2013). Improving the motion of a sensing antenna by using an input shaping technique. *ROBOT 2013. First Iberian Robotics Conference*, Madrid, Spain.

Huey, J. R., Sorensen, K. L., and Singhose, W.E. (2008). Useful applications of closed loop signal shaping controllers. *Control Engineering Practice*, 16(7), 836-846.

Kaneko, M., Kanayama, N., and Tsuji, T. (1998). Active antenna for contact sensing. *IEEE Transactions on Robotics and Automation*, 14(2), 278-291.

Park, J., and Chang, P. H. (2001). Learning input shaping technique for non-LTI systems. *ASME J. Dynamic Systems, Measur., and Control*, 123(2), 288-293.

Pearson, M.J., Mitchinson, B., Charles, S., Anthony, G., Prescott, P., and Tony, J. (2011). Biomimetic vibrissal sensing for robots. *Trans. R. Soc. B.* doi: 10.1098/rstb.2011.0164 366 2011.

Pereira, E., Trapero, J. R., Diaz, I. M. and Feliu, V. (2009). Adaptive input shaping for manoeuvring flexible structures using an algebraic identification technique. *Automatica*, 45(4), 1046-1051.

Prescott, T.J. and Pearson, M.J. (2009). Whisking with robots. *IEEE Robotics and Automation Magazine,* 16(3), 42-50.

Scholz, G.R., Rahn, C.D. (2004). Profile sensing with an actuated whisker. *IEEE Transactions on .Robotics and Automation*, 20(1), 124-127.

Singer, N. C., and Seering, W. C. (1990). Preshaping command inputs to reduce system vibration. *ASME J. Dynamics System, Measur., and.Control*, 112(1), 76-82.

Ueno, N., Kaneko, M., and Svinin, M. (1996). Theoretical and experimental investigation on dynamic active antenna. *IEEE International Conference of Robotics and Automation*, vol. 4, 3557-3563, Minneapolis, MN, USA.

Zhao, H. and Rahn, C.D. (2010). Repetitive learning control of a flexible whisker in tip contact with an unknown surface. *J.Vibration and Control*, 17(2), 197-203.